Electrochemical-driven green recovery of lithium, graphite and cathode from lithium-ion batteries using water

Abhishek Sarkar[1], Pranav Shrotriya[2], Ikenna C. Nlebedim[1,*]

1. Ames National Laboratory of US DOE, Ames, IA – 50011, USA
2. Department of Mechanical Engineering, Iowa State University, Ames, IA – 50011, USA

Abstract: The expected exponential increase in consumption of lithium-ion batteries (LIBs) would pose a unique challenge to the availability of near-critical resources like lithium and graphite in the upcoming decade. We present a lithium recovery process that utilizes a degradation mechanism, i.e., lithium plating, as a tool to concentrate metallic lithium at the anode/separator interface for convenient extraction at room temperature – using only water. Electrochemical characterization of fast charged (1 – 6 C) LIBs yielded a maximum capacity fade of 50% over ten cycles. The lithium plating was confirmed via voltage plateau analysis, coulombic efficiency, and DC resistance measurements. A maximum lithium plating condition was observed to exist between 4C and 5C, thereby limiting the energy consumption in the extraction process. Post-mortem film thickness measurement showed an incrementing film deposition with a maximum of 35µm thickness. SEM and XPS analysis confirmed increasing concentration of a dense dendritic metallic lithium deposition on the anode/separator interface with C-rate. A green recovery process was adopted to extract the concentrated metallic lithium using distilled water. The lithium from the plated film, solid/electrolyte interface (SEI), electrolyte, anode, and cathode, was extracted as salts. A 37% improvement in lithium recoverability was achieved with fast charging under ambient conditions. XPS analysis showed ~ 92% of lithium yield with no residual lithium in the graphite. In addition, the battery-grade graphite was recovered with 97% purity after heat treatment of the washed anode film, and concentrated transition metals oxides in the cathode to 93% purity for convenient extraction.

Keywords: Green recovery technology, Lithium extraction, Graphite recovery, Electrochemical lithium deposition.

1. Introduction

Lithium-based batteries represent ~37% of the rechargeable battery market with the highest product life and nearly 100% cycling efficiency, compared to other energy storage solutions (Swain, 2017). The global demand for cleaner transportation presents a significant prospect for increased use of lithium-ion batteries (LIBs) in the electrification of vehicles, with a projected production capacity increase from 455 GWh (2020) to 1447 GWh (2025) at CAGR of 26% (Yu and Sumangil, 2021). The production capacity is forecasted to exceed 6000 GWh by 2030 (Kane, 2022), with the demands for LIBs consuming >95% of the available global lithium reserve by the same year (Azevedo et al., 2022). Although the global production was 100,000 metric tons of lithium in 2021 (Garside, 2022), the steep growth in lithium demand creates high pressure on the available natural resources, and supply constraints may limit the production of LIBs in the future.

Commercial LIBs have approximately 4 – 8 wt.% of the electrode as lithium. Although extraction of lithium through recycling of used battery may help in this burgeoning demand, only 5% of the used batteries are recycled in the U.S. (Oberhaus, 2020). Of this small fraction being recycled, the primary focus is on the recovery of cobalt, nickel and other critical transition metals, while <1% of lithium is recycled (Graedel et al., 2011). The recovery of lithium from used battery is limited because the current lithium recycling processes consume significant fresh water and requires hazardous materials like acids, leading to environmental concerns (Coren, 2021). Additionally, the cost of lithium recovery far exceeds that of manufacturing batteries from natural resources (Beaudet et al., 2020). According to a Swedish Energy Agency report (Melin, 2019), the cost of recycling lithium is thrice that of obtaining lithium from natural sources. The current limited recovery of lithium via recycling, coupled with the increasing demand, will

exacerbate the criticality of Li and graphite in the very near future (Greim et al., 2020; Miatto et al., 2020; Watari et al., 2020). Of all anode materials, graphite is the most widely used (Chung, 2002) in commercial applications with a global market of almost US$1 billion in 2019 and projected market share of US$1.9 billion by 2024 (Chen, 2020; Sarkar et al., 2021). There is therefore a need for environmentally safe process with ability to recover and reintroduce the critical elements as high-quality battery-grade products at competitive prices, thereby accelerating decarbonization by reducing the need to extract from natural sources (Beaudet et al., 2020).

The two industrial approaches for recycling of LIBs are pyrometallurgy and hydrometallurgy (Kim et al., 2021; Liu et al., 2019; Steward et al., 2019; Swain, 2017). Pyrometallurgical recycling processes are the most common, and typically enable the extraction of aluminum, copper, and transition metals like cobalt, nickel, and manganese, from the batteries. However, this process incinerates the graphite, and the lithium is lost in the effluent slag as lithium hydroxide/oxide (Castillo et al., 2002; Dunn et al., 2012). The energy costs and the carbon footprint from operating the furnace make pyrometallurgical processes economically and environmentally inefficient. On the other hand, the hydrometallurgical processes involve reacting the spent cathode of LIBs in strong mineral acids (HCl, H_2SO_4, HNO_3) with/without a reducing agent (H_2O_2) to reduce and dissolve them in aqueous solution, followed by selective separation of the individual components (Golmohammadzadeh et al., 2017; Jha et al., 2013; Li et al., 2017). Since the LIBs are typically dismantled in a fully discharged state, the lithium is concentrated at the cathode which does not readily dissolve in water and requires an acidic medium for separation. Lithium extraction occurs either as the last step in the acid leaching process via successive co-precipitation of transition metals in alkaline medium, or by solvent extraction

methods (Chen et al., 2015; Li et al., 2017, 2010; Zhu et al., 2012). The hydrometallurgical process is efficient (> 99% Li) at an average operating temperature of 75℃, as summarized by Yao et al. (Yao et al., 2018). However, leaching at lower temperatures (< 50℃), decreases the efficiency due to slower reaction kinetics (Jha et al., 2013). Therefore, the process poses environmental concerns due to toxic emissions (Cl_2, SO_3, NO_x) (Sun and Qiu, 2012), waste management (Yao et al., 2018) and energy consumption (lower than pyrometallurgical processes). In addition, lithium may not be recovered from the electrolyte and/or the anode in both processes, due to the complications associated with hydrofluoric acid generation (Liu et al., 2019). Recent works have demonstrated the use of water as an efficient green solvent for separating cathode with residual lithium from aluminum (Fan et al., 2021).

We report an efficient and green method for selective extraction of Li from end-of-life secondary LIBs of any capacity and size under ambient conditions with no toxic emissions or effluents (Fig.1). The method enables the active lithium in the LIB to be concentrated on the anode/separator interface via electrochemical-driven lithium metal deposition (or lithium plating) by fast charging of the LIBs. In-situ electrochemical analysis and post-mortem film characterization are performed to monitor the lithium deposition. Subsequently, the plated Li is recovered by processing a dismantled battery with only distilled water. The lithium metal being more reactive than intercalated lithium, enables rapid dissolution and recovery at room temperature. The process not only enables the recovery of the plated lithium on the anode surface, but also enables recovery from the organic and inorganic salts in the solid electrolyte interphase (SEI) layers, (a term suggested by Peled (Peled, 1979)), and the electrolyte. In addition, the process substantially strips the cyclable Li from the cathode and concentrates it on the anode, hence reducing the complexity and cost of subsequent recovery processes for other

critical metals like cobalt, etc. from the cathode. After Li recovery from the anode, the battery-grade graphite is also recovered by heat treatment process. A significance of the proposed process lies in the ability to concentrate the Li onto the anode surface (even in a fully discharged state), allowing convenient and acid-free dissolution and recovery of Li.

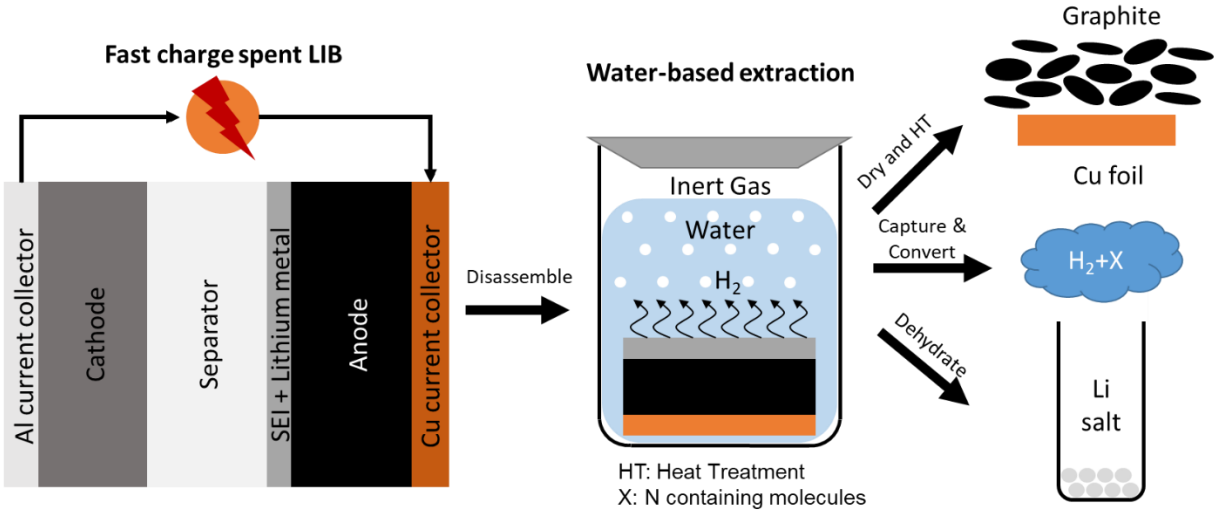

Figure 1. Schematic of lithium extraction and recovery via. electrochemical deposition.

2. Experimental

2.1. Electrochemical Analysis

Lithium cobalt oxide (LCO)/graphite (C) pouch cells (20mAh, Powerstream Inc.) were cycled using MTI BST300 8-channel battery charging station. The pouch cells were first discharged to 3.0V at a constant current (CC) of C/20 charging rate. A rest period of 30mins was introduced after every charge and discharge step to stabilize the electrochemical interactions within the electrodes. In the first cycle, the cells were charged to 90% state of charge at C/20 (CC) followed by a discharge to 3.0V at C/20 (CC). Following the slow cycle charge, fast charging was performed at desired C-rate (1 – 6 C, CC) till 4.2 V, followed by a constant voltage (CV) till approximately 90% state of charge. The cells were then discharged at C/2 (CC) till 3.0V. The

fast charging was repeated over 10 cycles. Finally, the pouch cells were fully discharged till 2.7V at 0.4C (CC) and followed by a CV till C/20 prior to dismantling.

2.2. Post-mortem analysis

The pouch cells were immediately transferred into a MBraun glovebox (<0.1ppm of H_2O and O_2), after being fully discharged. The cell casing was removed, and the jelly roll was carefully unfolded to avoid damaging the film deposited on the anode/separator interface. The film thickness measurements were performed using a Mitutoyo digital micrometer (Series 293 MDC-MX). Field emission scanning electron microscopy (FE-SEM) was performed on the anode surface with a FEI Teneo field emission scanning electron microscope. Samples were transferred using a vacuum transporter to avoid surface oxidation of the deposited Li film. The Li elemental analysis of the film was performed with X-ray Photoelectron Spectroscopy (XPS, Kratos Analytical, AMICUS XPS) and Electron Paramagnetic Resonance (EPR, ELEXSYS E580 FT-EPR) to detect Li metal deposition.

2.3. Materials recovery and characterization

The anode/separator (50.8mg/30.4mg) and cathode (172.9mg) were separately stored in different vials and transferred out of the glovebox. The elemental analysis of the electrode samples is provided in Results section. The samples were immediately introduced to 5mL of distilled water (large excess) under a fume hood and allowed to react for 3h. The solution (after removal of the electrode) was centrifuged for 10mins to precipitate and separate any insoluble electrode contamination. The pH and conductivity of the solution was measured at room temperature. Finally, the solution was dried for 48h at 80°C. The addition of water and subsequent drying of the anode film naturally de-bonded and liberated the graphite particles from the copper foil. The dried lithium salt, graphite and cathode film were analyzed using XPS. Inductively Coupled

Plasma Optical Emission Spectroscopy (ICP-OES, Agilent ICP-OES system) was performed on extracted and dried cathode (sans aluminum current collector) dissolved in 2M H_2SO_4 and 10% H_2O_2, followed by dilution with distilled water to ~ 10ppm (metal basis).

The extracted and dried graphite was heat treated in Ar flow (3scfh) under full vacuum (-760 mm Hg). The heat treatment protocol involved 10h ramp from 20℃ to 1000℃, 48h dwell at 1000℃ and 10h ramp down to 20℃. Raman spectroscopy was performed on the pre- and post-HT graphite anode samples by taking at least 3 spectral measurements to acknowledge the heterogeneity in the sample. To analyze the thermal transitions and stability of graphitization process, Thermogravimetric Analysis (TGA) with Differential Scanning Calorimetry (DSC) (Netzsch STA 449 F1 Jupiter) was performed. The sample was heated from 40℃ to 1000℃ at 10℃/min, 2h of dwell at 1000℃, ramp down to 40℃ at 10℃/min, and dwell for 30min at 40℃. The cycle was repeated twice to verify thermal stability of the heat-treated product after the first cycle.

3. Results and Discussion

During normal charging operation (< 1C charging rate) of a LIB, lithium ions would intercalate and store within the layers of a graphite electrode. The graphite electrode undergoes phase transitions from $LiC_{72} \rightarrow LiC_{36} \rightarrow LiC_{27} \rightarrow LiC_{18} \rightarrow LiC_{12} \rightarrow LiC_6$ with electrochemical potential plateauing at 210, 120 and 85 mV (vs. Li^+/Li), respectively (Ohzuku et al., 1993). The SEI formation/growth initiates at a potential window above 400 mV (vs. Li^+/Li) (Kasnatscheew et al., 2018; Zhang et al., 2001) for an $LiPF_6$-based electrolyte. However, the accelerated growth of the SEI layer occurs beyond 300 mV during charging, especially below 100 mV regime (Attia et al., 2019; Ota et al., 2004). However, fast charging of LIBs induces a large lithium flux on the anode/separator interface. The large ionic flux and diffusion limitation of the anode causes a

158 considerable increase in the lithium-ion concentration on the anode surface, resulting in the
159 anodic potential of < 0 V (vs. Li^+/Li, or < -3.05 V SHE). Under such circumstances, the anodic
160 potential range becomes thermodynamically favorable for metallic lithium to deposit over the
161 anode particles, in addition to intercalating with the electrode (Sarkar et al., 2020). This
162 phenomenon is commonly known as lithium plating which may start from moderate to higher
163 charging rates (C-rate > 1C) (Klein et al., 2021; Sarkar et al., 2022). The lithium metal
164 deposition can occur either dendritically or homogenously over the anode surface. After the
165 charging period, the anodic potential becomes positive, causing the metallic lithium to partially
166 strip off into the electrolyte in its ionic form. The stripped lithium ions either reversibly
167 intercalate into the anode, causing a plateau in the relaxation voltage profile (Petzl and Danzer,
168 2014), or irreversibly react with the solvent in the electrolyte to form an SEI film over the
169 deposited metallic lithium (Campbell et al., 2019; Gargh et al., 2021; Sarkar et al., 2020). A
170 considerable fraction of the metallic lithium gets passivated by the SEI film and stored at the
171 anode surface as dead lithium (Bitzer and Gruhle, 2014; Sarkar et al., 2021), thus accumulating
172 over the consequent fast charging cycles. The phenomena of lithium electrodeposition and dead
173 lithium storage via application of high charging currents over multiple cycles offers the ability to
174 accumulate Li for recycling via the proposed process.

175 The first cycle relaxation voltage analysis of the fast charged pouch cells (1 – 6 C) revealed a
176 plateau, indicating the plated lithium metal stripping (Fig.2a) after the charging half cycle. The
177 broadening of the voltage plateau indicated an increment in lithium stripping from 1C to 5C,
178 followed by decrease at 6C. The maximum lithium plating was found to occur between charging
179 rates 4C and 5C. For 1C to 3C and 6C, the voltage plateau relaxed completely within the resting
180 period, indicating complete re-intercalation was achieved by the battery during this period. For

4C and 5C, the voltage plateau did not diminish completely indicating incomplete re-intercalation during the rest period.

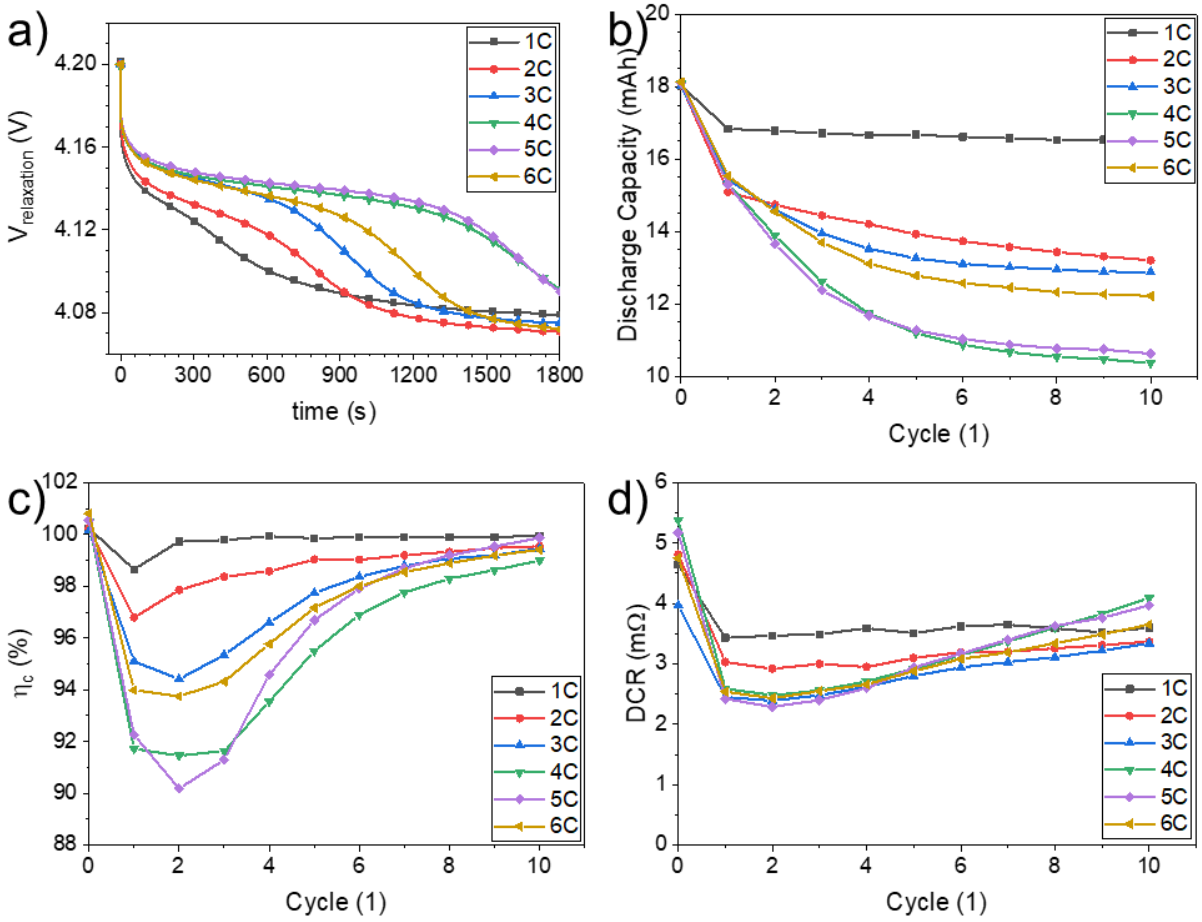

Figure 2. Electrochemical analysis of pouch cells fast charged from 1 – 6 C over 10 cycles, a) Voltage relaxation profile, b) Discharge capacity vs. cycle, c) Coulombic efficiency vs. cycles, and d) DC resistance (DCR) vs. cycles.

A saturation behavior was observed in the discharge capacity plot over multiple cycles (Fig.2b). The initial sharp capacity fade indicates rapid lithium loss from the electrolyte to be deposited as metallic lithium. The saturation of the discharge capacity indicated a suppression of the lithium deposition due to SEI formation over the plated lithium, especially at very high charging rates (C-rates) (> 5C). At 6C, the reduction in the voltage plateau (Fig.2a) and the increase in discharge capacity (Fig.2b) suggest a reduced lithium deposition, thereby limiting the current requirements for maximum lithium deposition to 5C. The reduced amount of plated lithium at 6C

is likely due to the significantly short charging times, minimizing the effective time to plate. A 50% loss in discharge capacity at 5C indicated that half of the cyclable lithium was concentrated onto the interfacial film for recovery.

The coulombic efficiency (Fig.2c) decreased sharply over the first few cycles, supporting the hypothesis of lithium plating from the capacity fade analysis. The observed increase in the efficiency with continuous cycling indicated a saturation in the plating mechanism beyond first couple of operating cycles (Burns et al., 2015). A decrease in the first cycle DCR measurements of the pouch cells (Fig.2d) attested to the deposition of conductive material within the pouch cell. The increasing cell resistance beyond the first few cycles further confirms the suppression of lithium plating mechanism.

Post-mortem thickness and mass evaluations showed an increase in film deposition till 5C, with a decay in the subsequent cycle (Fig.3). The film characteristics were determined by considering the thickness of a slow charged (C/20, Pristine) pouch cell anode as the baseline. The results support the observations from the in-situ electrochemical analysis and predict an optimum operating condition near 5C. An interesting observation was the magnitude of the deposited lithium film in Fig.3. Low temperature analysis (at ~ 1C) and modeling efforts (single cycle) have predicted a film thickness in the order of 100 – 1000 nm (Bitzer and Gruhle, 2014; Sarkar et al., 2020). However, the observed film thickness of >10µm (primarily due to ultrafast charging rates over multiple cycles) strongly improves the potential to recover lithium from LIBs.

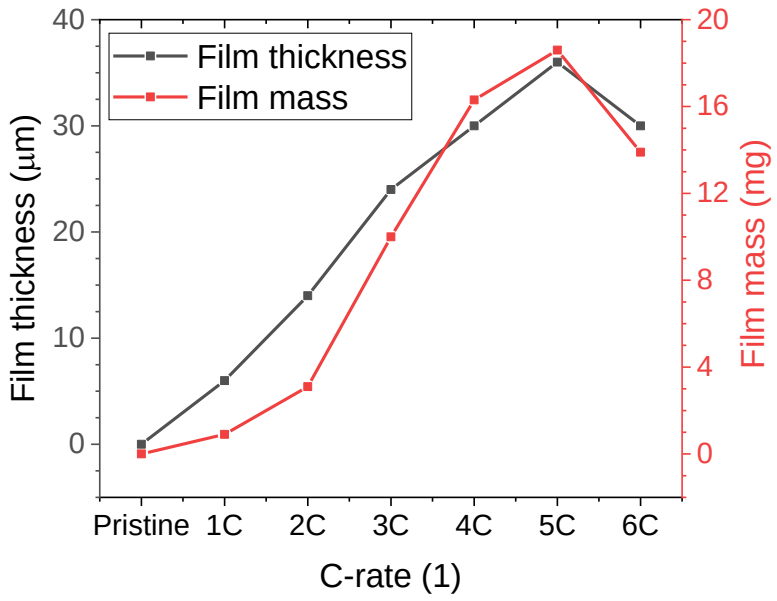

Figure 3. Anode film thickness and mass characterization vs. C-rate.

To further observe the morphology of the increasing lithium deposition on the anode surface at elevated charging rates, Field Emission Scanning Electron Microscopy (FE-SEM) analyses were performed on pristine, 1C, 3C and 5C samples (Fig.4). The micrograph of the pristine graphite anode shows an array of exfoliated graphite flakes with indications of a thin SEI film deposition, but with no lithium deposition (Fig.4a). For the sample cycled at 1C, dendritic depositions were observed to have initiated over the graphite flakes (Fig.4b). Others have also reported the same (Liu et al., 2016; Ren et al., 2019; Wang et al., 2017). A partial coverage of the deposited lithium was found at 1C, with clear visibility of the graphite flakes underneath. With increasing C-rate from 3C to 5C, an exponential increment in dendritic lithium plating was observed (Fig.4c, d). At 5C (Fig.4d), the surface morphology of the anode was completely dominated by metallic lithium whiskers with fault lines associated with film fracture from residual mechanical strain (Sarkar et al., 2020). Elemental and chemical analysis of these dendritic depositions were confirmed to be metallic lithium plating by XPS and Electron Paramagnetic Resonance (EPR) (Fig.S1). The XPS analysis shows a definitive Li metal peak at the surface of the 5C – 10 cycles

sample (Fig.S1a). Since XPS is a surface characterization tool with a penetration depth of ~ 10 nm, the small metal peak is a resultant of Li metal dendrites being covered by a dense SEI layer. To further support Li metal electrodeposition, EPR analysis of the anode with film deposition was undertaken. Li metal is strongly paramagnetic (Wandt et al., 2018) resulting in a large Dysonian peak. The EPR analysis confirms an increasing Li metal deposition with charging rate (Fig.S1b).

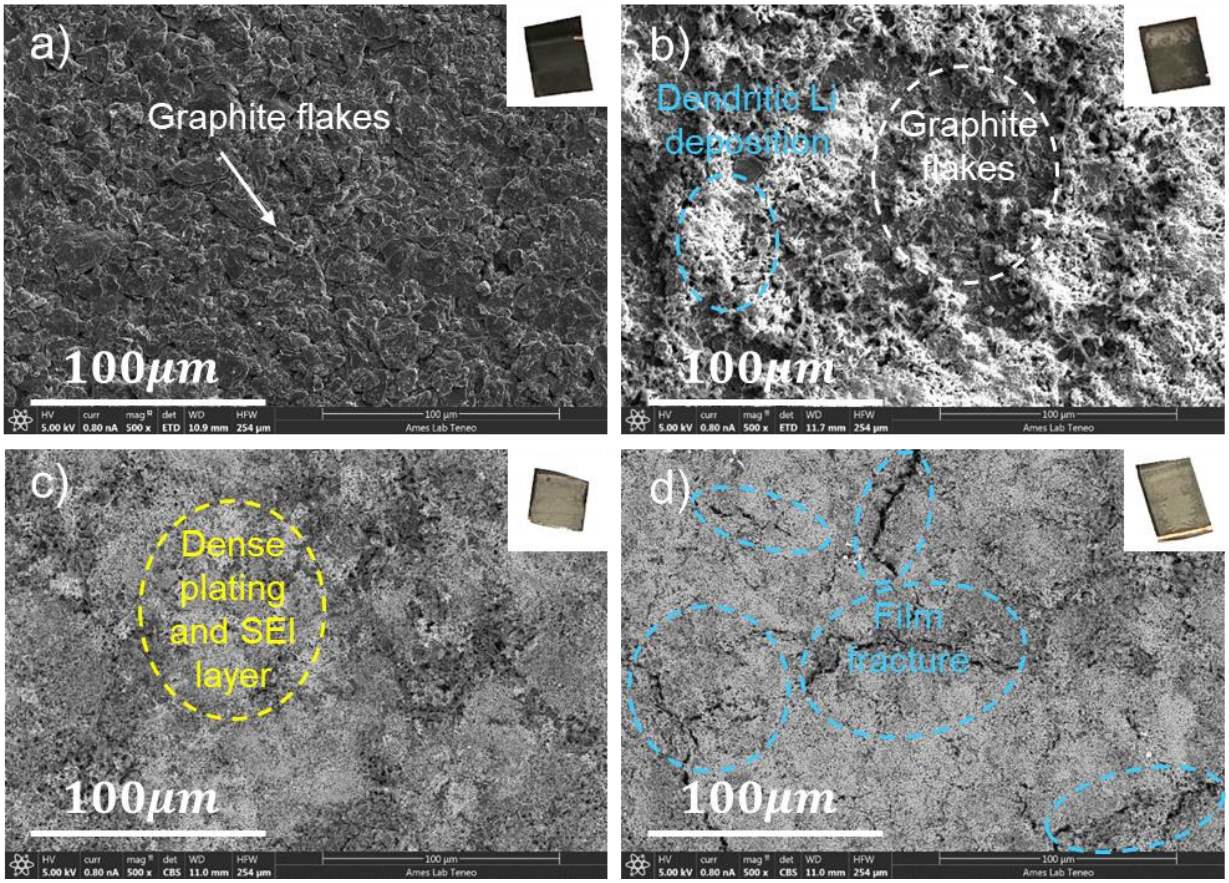

Figure 4. FE-SEM micrographs with optical images (subplot) of the anode surface with the film deposition, a) Pristine, b) 1C, c) 3C, and d) 5C.

The weight of extracted lithium salts from the anode/separator and cathode batches after the recovery and drying are shown in Fig.5. An increasing lithium deposition was observed with C-rate in the anode till a maximum (Fig.5a). This observation confirmed the upper charging limit to be between 4C and 5C, for the fresh LCO/C battery at room temperature and with a 37%

improvement in lithium recoverability. This condition could however vary for a used LIB depending on end-of-life condition or a different cathode chemistry and would need to be optimized during industrial adaption. For a pristine battery, the intercalated lithium would require thermal agitation (high temperature) to increase the amount of recoverable Li and a small quantity deposit as SEI. During the fast charging, the cyclable lithium is considerably lost from the cathode and the electrolyte and concentrated on the anode. A corresponding decrease in the lithium extraction was observed in the cathode (Fig.5b), indicating targeted concentration of metallic lithium at the anode/separator interface, which being more reactive than intercalated lithium enables efficient recovery under ambient conditions.

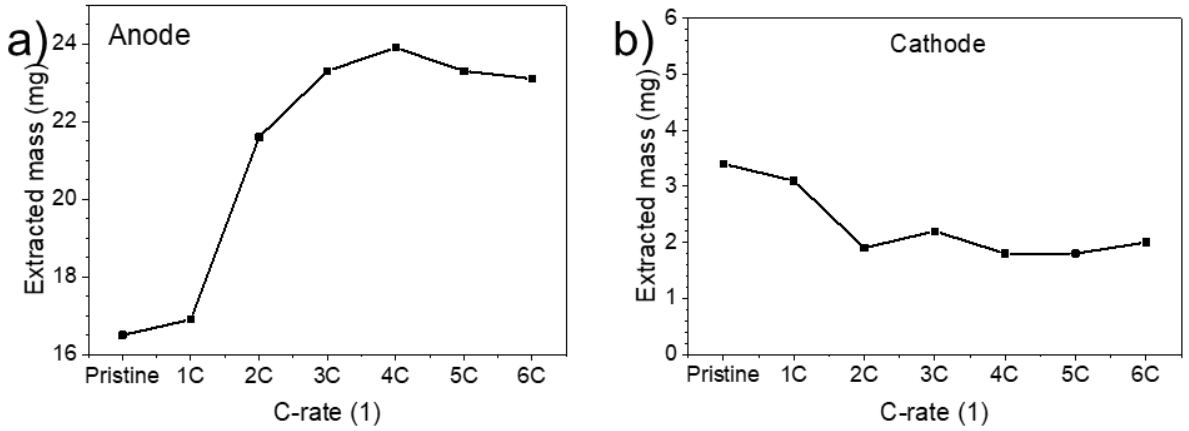

Figure 5. Extracted lithium salt gravimetric analysis vs. C-rate, a) Anode, and b) Cathode.

The lithium extraction process from the anode and the separator samples were done using distilled water. The metallic lithium (Li), the intercalated lithium (Li_xC_6, $x < 1$) in the graphite electrode and residual lithium in the cathode (Li_yCoO_2, $y < 1$) were extracted, as shown in the following chemical reactions.

$$2Li + 2H_2O \rightarrow 2LiOH + H_2 \quad (1)$$

$$Li_xC_6 + xH_2O \rightarrow xLiOH + 6C + \frac{x}{2}H_2 \quad (2)$$

$$Li_yCoO_2 + yH_2O \rightarrow yLiOH + CoO_2 + \frac{y}{2}H_2 \quad (3)$$

The electrolyte ($LiPF_6$) in the separator would decompose in contact with water to form hydrofluoric acid (HF). The HF would consecutively be consumed in decomposition of the SEI layer ($Li(RCHOCO_2)$).

$$LiPF_6 + H_2O \rightarrow LiPOF_4 + 2HF \quad (4)$$

$$LiPF_6 + 4H_2O \rightarrow LiF + 5HF + H_3PO_4 \quad (5)$$

$$2(RCHOCO_2)Li + 2HF \rightarrow 2LiF + (RCHOH)_2 + 2CO_2 \quad (6)$$

The lithium hydroxide (LiOH) thus produced could decompose, get carbonated and neutralize the excess HF and H_3PO_4, when in contact with atmosphere and the gases evolved from the SEI decomposition, in line with reactions 7 – 10.

$$2LiOH \rightarrow Li_2O + H_2O \quad (7)$$

$$2LiOH + CO_2 \rightarrow Li_2CO_3 + H_2O \quad (8)$$

$$LiOH + HF \rightarrow LiF + H_2O \quad (9)$$

$$3LiOH + H_3PO_4 \rightarrow Li_3PO_4 + 3H_2O \quad (10)$$

Therefore, the solution produced by adding water to the plated anode and the separator would primarily contain LiOH, Li_2O, Li_2CO_3, LiF, Li_3PO_4, and $LiOPF_4$. The pH and conductivity of the solution was measured (Fig.S2). A similar pattern was observed in the conductivity measurements as the electrochemical analysis (Fig.2), with the solution pH and conductivity was found to increase with C-rates. A key point to highlight from the pH measurements is the

alkaline nature of the extraction solution, indicating a complete neutralization of the HF formed in the process. The oscillations in the conductivity measurement occurred because the extracted solution contain other salts in addition to LiOH. The SEI and electrolyte decompose along with the plated lithium, consequently forming other lithium salts. In an ideal situation, only the lithium metal on the anode film would have dissolved in water to yield equivalent LiOH. The variability in the dissociation constants and solubility of the different lithium salts and their byproducts introduced the observed conductivity deviations with C-rate.

The lithium salts yielded from the battery are shown in Fig.6a. The 5C batch of the lithium salt was analyzed using XPS. The lithium peak from the XPS was deconvoluted and fitted with the above-mentioned lithium salts (Fig.6b). The peak areal analysis predicted about 50% of the salt composition was LiOH, followed by Li_2O, Li_2CO_3, LiF, $LiOPF_4$ and Li_3PO_4, respectively. This analysis confirmed that most of the lithium was derived from the electrodeposited layer. Since the pouch cell was completely discharged prior to disassembly, the contribution of LiOH from the intercalated graphite (Reaction 2) was assumed to be insignificant. Since the Li_2O and Li_2CO_3 (Reactions 7 and 8) were mostly generated as a byproduct of LiOH decomposition, the total metallic lithium contributed > 80% of the yield composition. The remainder of the yield were derived either from the SEI or the electrolyte decomposition. The extracted lithium salt may be heat treated with transition metal salts to form fresh battery electrodes.

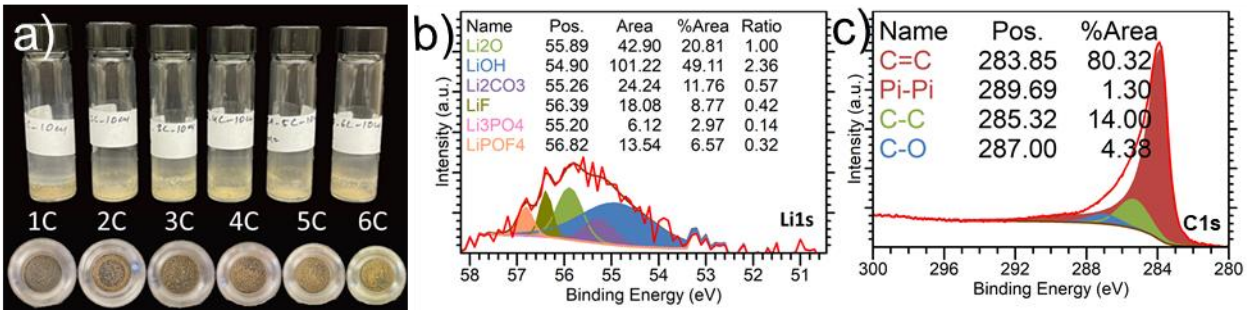

Figure 6. a) Lithium salt samples extracted from the pouch cells charged from 1 – 6 C, b) XPS L 1s deconvolution of lithium salt from the 5C batch, and c) XPS C 1s deconvolution of washed anode from 5C batch after extraction.

The molar concentrations from the XPS data were used to estimate an equivalent lithium extraction from the battery. For an initial yield of 23.3 mg of extracted salts, molar analysis presented in Table 1 indicates the presence of 5.53 mg of lithium (m_{Li}). With a 300 mg/Ah of lithium content in a lithium cobalt oxide battery (FedEx Express, 2020), the lithium yield from a 20 mAh (6 mg of Li) LCO/C pouch cell equates to ~92% of the lithium content. The flowchart of the entire process representing the salts in the extracted batch is presented in Fig.S3.

Table 1. Analysis of equivalent mass of extracted lithium determined from deconvolution of XPS lithium spectrum for 5C.

Compound	**Molar Mass (g/mol)**	**Molar Ratio (%)**	**Mass (mg)**	**n (mmol)**	**m_{Li} (mg)**
Li_2O	29.88	20.81	3.54	0.12	1.66
LiOH	23.95	49.11	6.70	0.28	1.96
Li_2CO_3	73.89	11.76	4.95	0.07	0.94
LiF	25.94	8.77	1.30	0.05	0.35
Li_3PO_4	115.79	2.97	1.96	0.02	0.36
$LiPOF_4$	129.91	6.57	4.86	0.04	0.26

The XPS deconvolution of the washed graphite (after lithium extraction) from the pouch cell revealed no trace of lithium (Table S1), indicating a complete lithium recovery from the anode. Moreover, the sample was found to be 89.9 at.% C1s. This result is further supported by the deconvolution of C 1s spectrum (Fig.6c). The analysis shows the C 1s within the washed anode was composed of 82.62 at.% graphite (283.85 eV), 14.00 at.% $C-C$ from the binder (285.32 eV) and 4.38 at.% of $C-O$ from electrolyte decomposition (Shchukarev and Korolkov, 2004). Carbon fluorine (C-F) species were not observed in the analysis. The extracted and dried graphite was heat treated (HT) in Ar flow under full vacuum and at 1000℃. A 30% mass loss was observed indicating decomposition of residual hydrocarbons from the filler and binder

materials. Post-HT XPS analysis revealed 7.65% increment in the elemental carbon content with C 1s of 96.8 at.% and 3.2 at.% of other elemental species. This indicated a reduction in the surface impurity on the graphite particles after the HT process. Raman spectra were obtained from the pre- and post-HT graphite anode samples (Fig.7a). The disorder peak (D band) was suppressed in the post-HT sample, inferring an increase in the graphitic behavior of the anode, and reduction in the amorphous filler and binding materials. The I_G/I_D ratio increased from 1.79 to 3.13 after the heat treatment process, indicating a 75% increase in the degree of graphitization. The post-HT graphite appears very similar to commercial battery-grade graphite. In addition, TGA and DSC analysis were performed to evaluate the thermal transitions and mass loss during the HT process of the graphite sample (Fig.7b). A two-stage mass loss is observed during the first cycle heating, with expected water removal by 300°C and decomposition of the binding material into carbon by 450°C. The second cycle iteration of the process revealed no significant mass or thermal changes, indicating a stable product with no further thermal decompositions up to 1000°C. We are currently optimizing the HT process to enable enhanced extraction of graphite and the results will be reported in future.

Compositional analysis of the untreated $LiCoO_2$ sample was performed using Inductively Coupled Plasma Optical Emission Spectroscopy (ICP-OES) (Table S2), indicating 41.5 at.% of Li and rest as Co (or $Li_{0.71}CoO_2$). The XPS deconvolution of the Co2p spectrum of the washed and dried cathode film was performed based on previous XPS measurements of Li_xCoO_2 electrodes at different states of charge (Dahéron et al., 2008; Dupin et al., 2001). The results, shown in Fig.7c, indicated < 10 at.% (or < 0.7 wt.%) of lithium. The deconvolution of the Li1s and Co3p peaks indicated 7.05 at.% of Li in CoO_2 structure (Table S2). Compositional analysis of the treated electrode was also performed with ICP-OES and revealed 7.77 at.% Li and the rest

92.95 at.% of Co (Table S2). These results agree within 1% of the amounts estimated from the XPS spectrum deconvolution. The XPS analysis of extracted Li (Fig. 6b and Table 1) showed 92.2 at.% recovery. The remaining 7.8 at.% of Li is present in material extracted from cathode as shown by XPS and ICP-OES. Therefore, for simple cathode chemistries, like lithium salts of cobalt oxide, manganese oxide and ferrous phosphate, the extraction process yields 93 at.% metal oxide/salts.

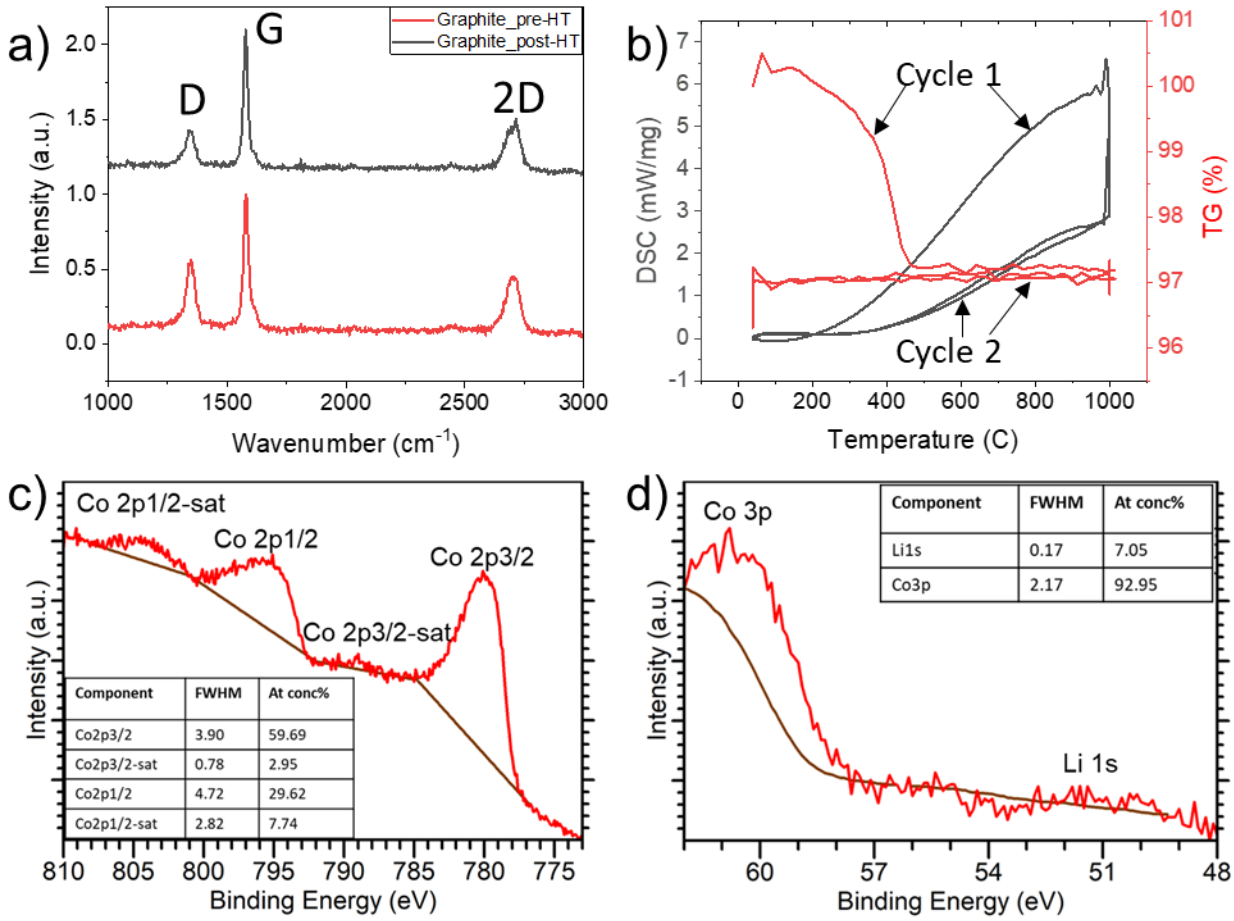

Figure 7. Graphite recovery via heat treatment of Li extracted anode, a) Raman spectra pf pre-HT and post-HT graphite, b) TGA and DSC of recovered graphite pre-HT. Cobalt oxide recovery from Li extracted cathode. XPS deconvolution of c) Co2p, and d) Li1s and Co3p.

H_2 evolution is a common feature of most hydrometallurgical processing with LIBs. Lithium either metal or intercalated in the cathode and anode would react with water (or any aqueous solution) to evolve H_2 (Equations 1 – 3) (McShane et al., 2020; Swain, 2017; YAMAGUCHI et

al., 2013). However, the evolved H_2 can be valorized. For each mole of Li, 0.5 mole of H_2 gas is evolved. A typical LIB has around 7 wt.% of Li, yielding 1wt.% of H_2, assuming 100% conversion. The recovery process could be performed under inert blanket (N_2) to prevent oxidation of the H_2. H_2 gas can be valorized as a heat source for drying the lithium solution and/or heat treating the extracted graphite. Hence the H_2 could be used as a clean fuel source to support the recovery process. In addition, future works would involve capturing the H_2 and converting it to value-added products, like urea or hydrides.

The lithium recovery process, thus, establishes four primary advantages, 1) ambient condition efficient recovery process due to high reactivity of lithium metal compared to intercalated lithium, 2) limited power requirement due to maximum lithium plating at 4 – 5 C, 3) environmental sustainability due to neutralization of HF produced and no additional acid requirement, and 4) recovery of lithium, graphite, and single transition metal oxide cathodes (CoO_2). A materials mass flow analysis was performed with the initial masses of anode (50.8 mg) and cathode (172.9 mg). The estimated recovered masses were Li (5.5 mg), graphite (43.8 mg with almost 98% purity) and CoO_2 (160m8 mg with 92% purity). During industrial adoption, the used LIBs could be fast charged in a thermally controlled system to avoid runaway. Consequently, the cells could be directly disassembled and submerged in water, thus eliminating the inert atmosphere disassembly process. In the future, the target is to improve the lithium recovery to ≥99%. We also target to use the mixed lithium salt from the recovery process and heat treat with cobalt salt for solid-state synthesis of $LiCoO_2$.

4. Conclusions

A novel recycling method was presented in which electrochemical cycling enables lithium concentration and subsequent efficient recovery of lithium, cobalt and graphite using only water

at room temperature. The process takes advantage of the degradation mechanisms from fast charging lithium battery, i.e., lithium plating, as a tool to selectively concentrate metallic lithium at the anode/separator interface. In-situ electrochemical analysis indicated an increasing lithium deposition with charging rate up till 5C, followed by a decay. The maximum lithium plating at 4 – 5 C for the analyzed pouch cells, limits the energy requirements for the extraction process. This optimum condition would vary depending on end-of-life condition of used LIBs. The film characterization during post-mortem analysis revealed a maximum film thickness of 35μm with increasing lithium spatial deposition with C-rate. A green recovery technology was employed by which the lithium from the plated film, SEI, and electrolyte were extracted using only distilled water. High extraction efficiency is possible because metallic lithium is significantly more reactive than intercalated lithium. A 37% gain in lithium recoverability was observed between the lithium harvested from the fast charging and pristine electrodes. XPS analysis of the extracted lithium salt indicated > 80% of the lithium was derived from the dendritic film, with a total extraction efficiency of > 90% at 5C. No traceable lithium was found in the anode and 7 at.% of lithium was found in the materials extracted from cathode. The technology has also demonstrated the recovery of battery-grade graphite with 97% purity and concentrated the cobalt oxide in the cathode to 93% purity for downstream processing, and is extendable to all cathode chemistries. The process is environmentally safe as the HF generated during electrolytic decomposition is consumed.

Author Contributions

Abhishek Sarkar contributed towards Investigation, Methodology, Formal analysis, Visualization, Writing - original draft, Writing - review & editing. Ikenna C. Nlebedim contributed towards Supervision, Formal analysis, Investigation, Writing - review & editing,

Funding acquisition. Pranav Shrotriya contributed towards Supervision, Formal analysis, Writing - review & editing, Investigation.

Conflict of Interest

There are no conflicts to declare.

Acknowledgement

This work was supported by the Department of Energy, Laboratory Directed Research and Development program at Ames National Laboratory. Ames National Laboratory is operated for the U.S. Department of Energy by Iowa State University of Science and Technology under Contract No. DE-AC02-07CH11358. We would like to acknowledge the support from Dr. Igor Slowing's and Dr. Emily Smith's groups at Iowa State University for ICP-OES and Raman spectroscopy, respectively.

References:

Attia, P.M., Das, S., Harris, S.J., Bazant, M.Z., Chueh, W.C., 2019. Electrochemical Kinetics of SEI Growth on Carbon Black: Part I. Experiments. J. Electrochem. Soc. 166, E97–E106. https://doi.org/10.1149/2.0231904jes

Azevedo, M., Baczynska, M., Hoffman, K., Krauze, A., 2022. Lithium mining: How new production technologies could fuel the global EV revolution [WWW Document]. McKinsey Co.

Beaudet, A., Larouche, F., Amouzegar, K., Bouchard, P., Zaghib, K., 2020. Key Challenges and Opportunities for Recycling Electric Vehicle Battery Materials. Sustainability 12, 5837. https://doi.org/10.3390/su12145837

Bitzer, B., Gruhle, A., 2014. A new method for detecting lithium plating by measuring the cell thickness. J. Power Sources 262, 297–302. https://doi.org/10.1016/j.jpowsour.2014.03.142

Burns, J.C., Stevens, D.A., Dahn, J.R., 2015. In-Situ Detection of Lithium Plating Using High Precision Coulometry. J. Electrochem. Soc. 162, A959–A964. https://doi.org/10.1149/2.0621506jes

Campbell, I.D., Marzook, M., Marinescu, M., Offer, G.J., 2019. How Observable Is Lithium Plating? Differential Voltage Analysis to Identify and Quantify Lithium Plating Following Fast Charging of Cold Lithium-Ion Batteries. J. Electrochem. Soc. 166, A725–A739. https://doi.org/10.1149/2.0821904jes

Castillo, S., Ansart, F., Laberty-Robert, C., Portal, J., 2002. Advances in the recovering of spent lithium battery compounds. J. Power Sources. https://doi.org/10.1016/S0378-7753(02)00361-0

Chen, J., 2020. Graphite, Silicon, Metal, and Other Anode Materials for Motive Lithium-Ion Batteries: Global Market and Emerging Opportunities. Massachusetts.

Chen, X., Chen, Y., Zhou, T., Liu, D., Hu, H., Fan, S., 2015. Hydrometallurgical recovery of metal values from sulfuric acid leaching liquor of spent lithium-ion batteries. Waste Manag. https://doi.org/10.1016/j.wasman.2014.12.023

Chung, D.D.L., 2002. Review Graphite. J. Mater. Sci. 37, 1475–1489. https://doi.org/https://doi.org/10.1023/A:1014915307738

Coren, M.J., 2021. Electric cars are fueling the US's lithium mining boom [WWW Document]. Quartz.

Dahéron, L., Dedryvère, R., Martinez, H., Ménétrier, M., Denage, C., Delmas, C., Gonbeau, D., 2008. Electron Transfer Mechanisms upon Lithium Deintercalation from LiCoO 2 to CoO 2 Investigated by XPS. Chem. Mater. 20, 583–590. https://doi.org/10.1021/cm702546s

Dunn, J.B., Gaines, L., Barnes, M., Sullivan, J., Wang, M., 2012. Material and energy flows in the materials production, assemble, and end-of-life stages of the automotive lithium-ion battery life cycle.

Dupin, J.C., Gonbeau, D., Benqlilou-Moudden, H., Vinatier, P., Levasseur, A., 2001. XPS analysis of new lithium cobalt oxide thin-films before and after lithium deintercalation. Thin Solid Films. https://doi.org/10.1016/S0040-6090(00)01802-2

Fan, M., Chang, X., Guo, Y.-J., Chen, W.-P., Yin, Y.-X., Yang, X., Meng, Q., Wan, L.-J., Guo, Y.-G., 2021. Increased residual lithium compounds guided design for green recycling of spent lithium-ion cathodes. Energy Environ. Sci. 14, 1461–1468. https://doi.org/10.1039/D0EE03914D

FedEx Express, 2020. LITHIUM BATTERY CALCULATIONS [WWW Document].

Gargh, P., Sarkar, A., Lui, Y.H., Shen, S., Hu, C., Hu, S., Nlebedim, I.C., Shrotriya, P., 2021. Correlating capacity fade with film resistance loss in fast charging of lithium-ion battery. J. Power Sources 485, 229360. https://doi.org/10.1016/j.jpowsour.2020.229360

Garside, M., 2022. Global lithium mine production 2010-2021.

Golmohammadzadeh, R., Rashchi, F., Vahidi, E., 2017. Recovery of lithium and cobalt from spent lithium-ion batteries using organic acids: Process optimization and kinetic aspects. Waste Manag. 64, 244–254. https://doi.org/10.1016/j.wasman.2017.03.037

Graedel, T.E., Allwood, J., Jean-Pierre Birat, Arcelor-Mittal, Buchert, M., Hageluken, C., Reck, B.K., Sibley, S.F., 2011. UNEP Recycling rates of metals - A Status Report, a Report of the Working Group on the Global Metal Flows to the international Resource Panel, Group.

Greim, P., Solomon, A.A., Breyer, C., 2020. Assessment of lithium criticality in the global energy transition and addressing policy gaps in transportation. Nat. Commun. 11, 4570. https://doi.org/10.1038/s41467-020-18402-y

Jha, M.K., Kumari, A., Jha, A.K., Kumar, V., Hait, J., Pandey, B.D., 2013. Recovery of lithium and cobalt from waste lithium ion batteries of mobile phone. Waste Manag.

https://doi.org/10.1016/j.wasman.2013.05.008

Kane, M., 2022. Forecast: Li-Ion Battery Market Might Exceed 6 TWh/Year By 2030 [WWW Document]. INSIDEEVs.

Kasnatscheew, J., Wagner, R., Winter, M., Cekic-Laskovic, I., 2018. Interfaces and Materials in Lithium Ion Batteries: Challenges for Theoretical Electrochemistry. Top. Curr. Chem. 376, 16. https://doi.org/10.1007/s41061-018-0196-1

Kim, S., Bang, J., Yoo, J., Shin, Y., Bae, J., Jeong, J., Kim, K., Dong, P., Kwon, K., 2021. A comprehensive review on the pretreatment process in lithium-ion battery recycling. J. Clean. Prod. 294, 126329. https://doi.org/10.1016/j.jclepro.2021.126329

Klein, S., Bärmann, P., Stolz, L., Borzutzki, K., Schmiegel, J.-P., Börner, M., Winter, M., Placke, T., Kasnatscheew, J., 2021. Demonstrating Apparently Inconspicuous but Sensitive Impacts on the Rollover Failure of Lithium-Ion Batteries at a High Voltage. ACS Appl. Mater. Interfaces 13, 57241–57251. https://doi.org/10.1021/acsami.1c17408

Li, H., Xing, S., Liu, Y., Li, F., Guo, H., Kuang, G., 2017. Recovery of Lithium, Iron, and Phosphorus from Spent LiFePO4 Batteries Using Stoichiometric Sulfuric Acid Leaching System. ACS Sustain. Chem. Eng. https://doi.org/10.1021/acssuschemeng.7b01594

Li, L., Ge, J., Chen, R., Wu, F., Chen, S., Zhang, X., 2010. Environmental friendly leaching reagent for cobalt and lithium recovery from spent lithium-ion batteries. Waste Manag. https://doi.org/10.1016/j.wasman.2010.08.008

Liu, C., Lin, J., Cao, H., Zhang, Y., Sun, Z., 2019. Recycling of spent lithium-ion batteries in view of lithium recovery: A critical review. J. Clean. Prod. 228, 801–813. https://doi.org/10.1016/j.jclepro.2019.04.304

Liu, Q., Du, C., Shen, B., Zuo, P., Cheng, X., Ma, Y., Yin, G., Gao, Y., 2016. Understanding undesirable anode lithium plating issues in lithium-ion batteries. RSC Adv. 6, 88683–88700. https://doi.org/10.1039/c6ra19482f

McShane, E.J., Colclasure, A.M., Brown, D.E., Konz, Z.M., Smith, K., McCloskey, B.D., 2020. Quantification of Inactive Lithium and Solid–Electrolyte Interphase Species on Graphite Electrodes after Fast Charging. ACS Energy Lett. 5, 2045–2051. https://doi.org/10.1021/acsenergylett.0c00859

Melin, H.E., 2019. State-of-the-art in reuse and recycling of lithium-ion batteries – A research review.

Miatto, A., Reck, B.K., West, J., Graedel, T.E., 2020. The rise and fall of American lithium. Resour. Conserv. Recycl. https://doi.org/10.1016/j.resconrec.2020.105034

Oberhaus, D., 2020. The Race To Crack Battery Recycling—Before It's Too Late [WWW Document]. Wired.

Ohzuku, T., Iwakoshi, Y., Sawai, K., 1993. Formation of Lithium-Graphite Intercalation Compounds in Nonaqueous Electrolytes and Their Application as a Negative Electrode for a Lithium Ion (Shuttlecock) Cell. J. Electrochem. Soc. 140, 2490–2498. https://doi.org/10.1149/1.2220849

Ota, H., Sakata, Y., Inoue, A., Yamaguchi, S., 2004. Analysis of Vinylene Carbonate Derived SEI Layers on Graphite Anode. J. Electrochem. Soc. 151, A1659.

https://doi.org/10.1149/1.1785795

Peled, E., 1979. The Electrochemical Behavior of Alkali and Alkaline Earth Metals in Nonaqueous Battery Systems—The Solid Electrolyte Interphase Model. J. Electrochem. Soc. 126, 2047. https://doi.org/10.1149/1.2128859

Petzl, M., Danzer, M.A., 2014. Nondestructive detection, characterization, and quantification of lithium plating in commercial lithium-ion batteries. J. Power Sources 254, 80–87. https://doi.org/10.1016/j.jpowsour.2013.12.060

Ren, X., Zou, L., Cao, X., Engelhard, M.H., Liu, W., Burton, S.D., Lee, H., Niu, C., Matthews, B.E., Zhu, Z., Wang, C., Arey, B.W., Xiao, J., Liu, J., Zhang, J.-G., Xu, W., 2019. Enabling High-Voltage Lithium-Metal Batteries under Practical Conditions. Joule 3, 1662–1676. https://doi.org/10.1016/j.joule.2019.05.006

Sarkar, A., Nlebedim, I.C., Shrotriya, P., 2020. Performance degradation due to anodic failure mechanisms in lithium-ion batteries. J. Power Sources 229145. https://doi.org/10.1016/j.jpowsour.2020.229145

Sarkar, A., Shrotriya, P., Nlebedim, I.C., 2022. Anodic Interfacial Evolution in Extremely Fast Charged Lithium-Ion Batteries. ACS Appl. Energy Mater. 5, 3179–3188. https://doi.org/10.1021/acsaem.1c03803

Sarkar, A., Shrotriya, P., Nlebedim, I.C., 2021. Magnetohydrodynamic Control of Interfacial Degradation in Lithium-Ion Batteries for Fast Charging Applications. ACS Appl. Mater. Interfaces acsami.1c10788. https://doi.org/10.1021/acsami.1c10788

Shchukarev, A., Korolkov, D., 2004. XPS Study of group IA carbonates. Open Chem. 2, 347–362. https://doi.org/10.2478/BF02475578

Steward, D., Mayyas, A., Mann, M., 2019. Economics and Challenges of Li-Ion Battery Recycling from End-of-Life Vehicles. Procedia Manuf. 33, 272–279. https://doi.org/10.1016/j.promfg.2019.04.033

Sun, L., Qiu, K., 2012. Organic oxalate as leachant and precipitant for the recovery of valuable metals from spent lithium-ion batteries. Waste Manag. 32, 1575–1582. https://doi.org/10.1016/j.wasman.2012.03.027

Swain, B., 2017. Recovery and recycling of lithium: A review. Sep. Purif. Technol. https://doi.org/10.1016/j.seppur.2016.08.031

Wandt, J., Jakes, P., Granwehr, J., Eichel, R.-A., Gasteiger, H.A., 2018. Quantitative and time-resolved detection of lithium plating on graphite anodes in lithium ion batteries. Mater. Today 21, 231–240. https://doi.org/10.1016/j.mattod.2017.11.001

Wang, S.-H., Yin, Y.-X., Zuo, T.-T., Dong, W., Li, J.-Y., Shi, J.-L., Zhang, C.-H., Li, N.-W., Li, C.-J., Guo, Y.-G., 2017. Stable Li Metal Anodes via Regulating Lithium Plating/Stripping in Vertically Aligned Microchannels. Adv. Mater. 29, 1703729. https://doi.org/10.1002/adma.201703729

Watari, T., Nansai, K., Nakajima, K., 2020. Review of critical metal dynamics to 2050 for 48 elements. Resour. Conserv. Recycl. 155, 104669. https://doi.org/10.1016/j.resconrec.2019.104669

YAMAGUCHI, S., NAKAMURA, N., YAMAMOTO, H., INOKAWA, H., ICHIKAWA, T.,

KOJIMA, Y., MIYAOKA, H., 2013. Thermochemical Water-splitting Reaction by Alkali Metal-Cobalt Oxide. J. Japan Inst. Energy 92, 909–912. https://doi.org/10.3775/jie.92.909

Yao, Y., Zhu, M., Zhao, Z., Tong, B., Fan, Y., Hua, Z., 2018. Hydrometallurgical Processes for Recycling Spent Lithium-Ion Batteries: A Critical Review. ACS Sustain. Chem. Eng. 6, 13611–13627. https://doi.org/10.1021/acssuschemeng.8b03545

Yu, A., Sumangil, M., 2021. Top electric vehicle markets dominate lithium-ion battery capacity growth [WWW Document]. S&P Glob. Mark. Intell.

Zhang, S., Ding, M.S., Xu, K., Allen, J., Jow, T.R., 2001. Understanding Solid Electrolyte Interface Film Formation on Graphite Electrodes. Electrochem. Solid-State Lett. 4, A206. https://doi.org/10.1149/1.1414946

Zhu, S.G., He, W.Z., Li, G.M., Zhou, X., Zhang, X.J., Huang, J.W., 2012. Recovery of Co and Li from spent lithium-ion batteries by combination method of acid leaching and chemical precipitation. Trans. Nonferrous Met. Soc. China (English Ed. https://doi.org/10.1016/S1003-6326(11)61460-X